Geological Society, London, Special Publications

End-member modelling as an aid to diagnose remagnetization: a brief review

Mark J. Dekkers

Geological Society, London, Special Publications 2012, v.371; p253-269.
doi: 10.1144/SP371.12

Notes

End-member modelling as an aid to diagnose remagnetization: a brief review

MARK J. DEKKERS

Department of Earth Sciences, Paleomagnetic Laboratory 'Fort Hoofddijk', Faculty of Geoscience, Utrecht University, Budapestlaan 17, 3584 CD Utrecht, The Netherlands (e-mail: m.j.dekkers@uu.nl)

Abstract: Remagnetization of a palaeomagnetic signal is difficult to recognize independently of directional information. The situation becomes more complex when remagnetized rocks pass palaeomagnetic field tests, for example when the remagnetization of a rock sequence has occurred before folding. It is evident that palaeogeographic reconstructions are seriously flawed when actually remagnetized rocks are not identified as such. Here we discuss the merits and pitfalls of so-called end-member modelling of acquisition curves of the isothermal remanent magnetization (IRM) to recognize remagnetized strata. The technique requires no *a priori* information about the IRM acquisition curves. The algorithm unmixes a set of IRM acquisition curves into a number of invariant curves termed end members and calculates the mixing proportions of the end members for each sample. Since primary natural remanent magnetization (NRM) and remagnetized NRM are acquired by different processes, their signatures can be recognized from subtle differences in the magnetic properties. We illustrate the potential of the approach by three case studies, one from Spain and two from Turkey, in which the magnetic properties of remagnetized and non-remagnetized rocks are evaluated.

The natural remanent magnetization (NRM) of a rock is described as remagnetized when it represents a palaeomagnetically younger age than the sediment age of the rock formation under study. Remagnetization interferes with palaeogeographic reconstructions, as is increasingly being appreciated. The 'Late Palaeozoic remagnetization event' was firmly recognized in the Appalachians in the USA in the early 1980s (e.g. McCabe *et al.* 1983; see the review of Van der Voo & Torsvik 2012) while the implications of late Palaeozoic remagnetization in European counterparts, for example the Rhenohercynian belt and the Cantabrian mountain chain in Spain, were fully realized about a decade later (e.g. Molina Garza & Zijderveld 1996; Van der Voo *et al.* 1997; Weil *et al.* 2000; Weil & Van der Voo 2002; Zwing *et al.* 2002, 2009; Zegers *et al.* 2003). Yet remagnetization does not appear to be restricted to certain time periods in certain regions. Remagnetized rocks are being documented in rocks of all geological ages – including very young rocks – in orogenic belts and forelands across the entire globe. It can occur any time during the geological history, during either pre-folding (e.g. Perroud & Van der Voo 1984), syn-folding (e.g. Kent & Opdyke 1985) or post-folding (e.g. Stearns & Van der Voo 1987). It should therefore be tested whether or not a certain rock unit is remagnetized despite passing palaeomagnetic field tests. Remagnetized rocks obviously cannot be used for classic palaeogeographic reconstruction, a considerable disadvantage that has led to serious disappointment. However, the remagnetization process can offer geological information that is difficult to acquire otherwise. This includes spatial and temporal delineation of (approximate) palaeotemperatures that can be tied to maturation histories of potential hydrocarbon source rocks (Font *et al.* 2006) and the definition of 'remagnetized aureoles' that may indicate telethermal ore bodies, for example, Pb–Zn Mississippi Valley Type ores. Further, temporally slightly different remagnetization events could be demonstrated for several Iberian Mesozoic sedimentary basins, linked to the Aptian rotation of Iberia during a series of basin remagnetizations (Gong *et al.* 2009*a*).

While thermoviscous resetting (Kent 1985) is a plausible scenario to explain remagnetization processes in a number of occasions, in many other situations the rocks have never been heated for a sufficient amount of time at a sufficiently elevated temperature to make this mechanism viable. Grain growth at low temperature, (far) below the magnetic ordering temperature of the magnetic particles involved, assisted by fluids which are either internally buffered or externally derived, is the currently prevailing mechanism to explain remagnetization (e.g. McCabe & Elmore 1989; Elmore *et al.* 2006). The role of tectonic stress which is sometimes advocated (e.g. Evans *et al.* 2003; Evans & Elmore 2006; Oliva-Urcia *et al.* 2008; Zwing *et al.* 2009) is rather elusive. Substantial effort has gone into the visualization of magnetic particles

From: Elmore, R. D., Muxworthy, A. R., Aldana, M. M. & Mena, M. (eds) 2012. *Remagnetization and Chemical Alteration of Sedimentary Rocks*. Geological Society, London, Special Publications, **371**, 253–269.
First published online August 22, 2012, http://dx.doi.org/10.1144/SP371.12

by scanning and transmission electron microscopy that are argued to carry the remagnetization (e.g. Suk *et al.* 1993; Sun & Jackson 1994). Rocks that are considered to be remagnetized by a chemical remanent magnetization (CRM) contain abundant very small particles, straddling the nominally superparamagnetic (SP) to the single-domain (SD) size range. The focus of this contribution is on remagnetizations residing in magnetite, but remagnetizations that resides in greigite are also possible (e.g. Rowan & Roberts 2006, 2008).

Ideally, we would have criteria at hand to recognize remagnetization without the need to use palaeomagnetic directional information. In this case, a researcher could identify remagnetized rocks on the basis of their magnetic properties. The identification of the 'remagnetized' and 'non-remagnetized' trends based on hysteresis parameters plotted on a Day plot (Day *et al.* 1977) is an example of this approach (Channell & McCabe 1994). Modelling of SP particles on the Day plot (Dunlop 2002*a*, *b*; Lanci & Kent 2003) indeed shows positions on the Day plot perfectly compatible with the remagnetized and non-remagnetized trends of Channell & McCabe (1994). However, in a large number of studies (e.g. Zegers *et al.* 2003), actually measured hysteresis parameters appear to plot in between the two trend lines complicating the interpretation in terms of remagnetization. This could be due to mixed magnetic mineralogy not accounted for in Day plots or to actual contributions from a detrital component and a remagnetized component, leading to positions on the Day plot between the two trend lines. Further, for weakly magnetic rocks, it is not always straightforward to determine meaningful hysteresis parameters because of low signals despite the very sensitive instrumentation available. The correction of the high-field slope of the hysteresis loop becomes critical in cases of a small ferromagnetic (*sensu lato*) contribution and a large paramagnetic contribution.

Acquisition curves of isothermal remanent magnetization (IRM) can always be measured faithfully so that limit-of-detection problems inherent to hysteresis loop measurement are avoided. In remagnetization studies, we are primarily interested in the remanence carriers and so a remanence-based criterion to recognize remagnetization, for example an IRM-based criterion, would be preferable. In addition, chemical remagnetization adds magnetic particles to an existing particle suite in a rock often without actually replacing it. This follows from the notion that it is very difficult to envisage that fine-grained diagenetic magnetite would precipitate while coarser-grained detrital magnetite would dissolve at the same time. However, in cases where the sequence of rocks has undergone an 'intermediate' diagenetic greigite formation phase (e.g. Rowan *et al.* 2009), the originally present detrital magnetite could have been (largely) reductively dissolved before the later precipitation of diagenetic magnetite. In the cases discussed here greigite has not been determined, but it cannot be excluded at this stage that the diagenetic magnetite could be a product of greigite reactions. The resulting magnetic properties of a remagnetized rock sequence can be considered a composite of two processes: (1) detrital deposition/early biogenic formation and (2) later diagenetic formation, with the former potentially partially leached from the rock. These are often difficult to untangle by hysteresis parameter analysis.

It may be clear that in chemically remagnetized rocks the original 'detrital' NRM and the remagnetized NRM are acquired by very different processes that have led to different magnetic particle distributions. Such differences can be measured by means of detailed IRM acquisition curves. Since pervasive remagnetization is anticipated to have acted to a variable extent on a collection of samples, it is mathematically possible to unmix or decompose a collection of IRM acquisition curves into two or more invariant IRM acquisition curves termed end members (e.g. Weltje 1997; Heslop & Dillon 2007). All measured IRM acquisition curves are then expressed as the result of mixing of those end members. Here we briefly summarize the principles of the end-member unmixing algorithm of Weltje (1997) and demonstrate the potential of the end-member modelling approach to diagnose remagnetized rocks. It should be realized that a purely thermoviscous resetting of the NRM cannot be assessed with this technique because the grain-size distribution is not changed. However, in hydrous pro-grade high-diagenetic temperature regimes or very low-grade anchimetamorphic conditions in sediments it is hard to conceive that there would be no changes in the grain-size distribution of the magnetic particles as a result of diagenesis and metamorphism.

End-member modelling

End-member modelling is an inverse mathematical technique, that is, the model is derived from (measured) data (in the present contribution a collection of IRM acquisition curves). The measured data are considered to be a linear mixture of a number of invariant constituent components termed end members. The mixing space or polytope is subject to a constant sum requirement (i.e. data must be expressed as proportions or percentages; compositional data fulfil this requirement, for the present case the input consists of normalized IRM acquisition curves) and mixing proportions should not be negative (Weltje 1997). The constant sum

requirement ensures that the mixing plane (in the case of three end members, a two-dimensional equilateral plane triangle) contains the composition vector tips of all samples in the hyperplane or simplex. End-member modelling is an example of so-called bilinear unmixing. Bilinear implies here that both the end-member properties as well as their mixing proportions in each individual sample are determined from the same measured dataset. In our ternary diagram, all compositions throughout the diagram can be generated by combining the vertices of the triangle. However, any combination of three invariant points that span the data hull (the space that is occupied by the data) can be used to this end. The end members are therefore not unique in the mathematical sense and a geologically/palaeomagnetically reasonable set of end members should be sought that are subsequently used to calculate the mixing proportions for individual samples.

If the mixing was perfect this would yield (in matrix notation)

$$\boldsymbol{X} = \boldsymbol{MB}$$

where $\boldsymbol{X}$ represents the measured data matrix, $\boldsymbol{M}$ the mixing proportions for each individual sample and $\boldsymbol{B}$ the invariant points, that is, the end members. Mixing proportions cannot be negative. In reality, mixing is always imperfect to some degree because of sampling and measurement errors. $\boldsymbol{X}$ is thought to consist of $\boldsymbol{X} = \boldsymbol{X}' - \mathbf{E}$ in the terminology of Weltje (1997) where $\boldsymbol{X}'$ is the ideal mixing system and $\boldsymbol{E}$ is the matrix of error terms. We therefore have:

$$\boldsymbol{X} = \boldsymbol{MB} + \boldsymbol{E}$$

There exists a range of strategies to unmix which depend on the *a priori* information available. If the number of end members and their composition are known in advance, the mixing proportions $\boldsymbol{M}$ can be calculated by solving a set of linear equations; this is referred to as linear unmixing. In the more general case of bilinear unmixing, both the end-member compositions $\boldsymbol{B}$ and mixing proportions $\boldsymbol{M}$ must be determined. In practice this implies determination of the number of end members q, their properties $\boldsymbol{B}$, the mixing proportions $\boldsymbol{M}$, the ideal mixing system $\boldsymbol{X}'$ and the error matrix $\boldsymbol{E}$ (Weltje 1997). As outlined by Weltje (1997), there exist various schemes to solve the bilinear unmixing problem and there is no unique solution since any end member would be appropriate (from a mathematical viewpoint) as long as it lies on the edge or outside the multivariate space spanned by the data points. Solving schemes that consider a convex hull approach are deemed to be the most realistic, but they are very sensitive to deviating samples or outliers: a convex hull around the data must contain all data points. Weltje (1997) developed an elegant algorithm that alleviates the convex hull criterion: it is accepted that some data points remain outside the calculated data hull. In this way the end-member solution is (much) less sensitive to outlying samples. They are not considered in the solution, which makes the solution more robust to describe general patterns, groupings or trends in the data.

The unmixing problem is solved in a two-stage fashion which has also been adopted in several other schemes. First, the mixing space is partitioned into $\boldsymbol{X}'$ and $\boldsymbol{E}$ for each number of end members q considered. For optimal $\boldsymbol{X}'$ and q, $\boldsymbol{X}'$ is then expressed as the product of $\boldsymbol{M}$ and $\boldsymbol{B}$. An exact solution does not exist and an 'optimal' solution is sought.

The idea is that we start from within the data hull by using the cluster centres obtained by probabilistic fuzzy *c*-means cluster analysis (Bezdek *et al.* 1984), guaranteed to lie within the data convex hull. Iteratively, the mixing polytope is enlarged by moving the end members in order to include an increasingly greater number of data points until either all data points are included or a stopping criterion for the algorithm is reached. End members as close as possible to the convex hull are calculated with this approach. Such end members have meaningful mixing proportions, easing the geological interpretation (it is 'easier' from a process viewpoint to explain silt by some fragmentation or winnowing of sand than to propose gross fragmentation of pebbles). Distant end members only yield very small mixing proportions to explain the observations, a situation that is undesirable from a geological interpretation point of view.

End-member modelling has been used rather extensively in sedimentology to unravel the contribution of various source areas of sediments (e.g. Weltje 1997; Prins *et al.* 2002). Other examples include colour spectra that have been unmixed into end members to provide an interpretation in terms of provenance area and diagenetic processes off the coast of Africa (Heslop *et al.* 2007). Magnetic properties, that is IRM acquisition curves, have also been unmixed (e.g. Heslop & Dillon 2007), again to shed light on provenance areas and diagenetic processes.

Typically, at least 30–50 input curves should be used to achieve a reasonable picture of the inherent data variability. The end-member modelling algorithm aims to 'fill' the mixing space (in the case of three end members, the equilateral plane triangle) as evenly as possible. As stated earlier, both the shape of the end members and their abundances are based on the variation in the measured dataset that serves as input of the end-member model effort. There are no criteria concerning the shape

of the input curves, such as basis functions or type curves as in forward modelling techniques. The only constraints on the input data is that each input curve – here IRM acquisition curves – must be monotonic (i.e. each IRM value is greater than or equal to the foregoing measurement at a lower acquisition field) and must contain the same number of data points, each with the same set of *B*-values (or *H*-values; i.e. the IRM acquisition fields). Before the end-member model can be calculated, pre-processing of input IRM acquisition curves may be required (i.e. interpolation on to the same set of field values and forcing the IRM acquisition curves to be monotonic).

The end-member unmixing approach has a huge potential which we hope to outline in this contribution. However, it also has potential pitfalls. Since (almost) everything is possible, the user must have a certain idea of the significance of potential end members. The solution is mathematically non-unique and the most reasonable geological solution should be targeted (cf. Weltje 1997). The IRM acquisition curves are normalized to take out concentration effects (that can be visualized by back-transformation of the mixing proportions calculated). The input data are so-called closed data with their q end members forming the apices of a $q-1$-dimensional hyperplane or simplex (Weltje 1997). In the case of three end members, these are the apices of an equilateral plane triangle. Magnetic interaction could bias the linear additivity of the mixing of IRM components. However, for the dilute 'magnetic suspensions' (i.e. magnetic particles dispersed at low concentration in a rock sample) of interest here, magnetic interaction has been shown to be insignificant (Heslop *et al.* 2006; Heslop & Dillon 2007). It is also important to realize that the end members need not be unimodal coercivity distributions. If magnetite (*sensu lato*) and hematite (*sensu lato*) co-vary throughout a sample collection, they could be captured as a single end member. The end members reflect processes rather than specific magnetic minerals. However, for an in-depth understanding of the processes involved, knowledge of the magnetic mineralogy that makes up the end-members is a distinct advantage. End-member modelling is therefore often used in conjunction with (independent) forward modelling techniques to unmix individual IRM acquisition curves.

The optimal number of end members

Determining the number of meaningful end members which should be considered is at the heart of any end-member model interpretation. There exist various ways to calculate end members and related mixing proportions for a given dataset. By non-negative matrix factorization, the closest mixing polytope around the entire data hull is calculated iteratively. This makes the approach rather outlier-sensitive (one deviating input data curve can have an overly large influence). Iterative schemes that start from extreme observations also appear to be outlier-sensitive. If we start from within the convex hull of the data and iteratively expand the mixing polytope, the final solution is much less sensitive to outliers; this is especially true if we accept that not all data points must lie within the final mixing polytope (Weltje 1997). The effectiveness of the end-member model under consideration is evaluated from a mathematical viewpoint, primarily by the convexity error and the coefficient of determination.

The mismatch between the calculated end-member model and an ideal model that includes all data points is given by the so-called convexity error (Weltje 1997). This is determined by evaluating the location of the data points outside the mixing polytope. The convexity error conveys a measure of that mismatch by adding the logarithms of the proportion (Prop) of the samples outside the mixing polytope and of their mean-squared distance (Dist): $\log(\text{Prop}) + \log(\text{Dist})$. As an example, when 1% (0.01) of the observations are outside the mixing polytope and their average end-member contribution is −10% (0.1 thus squared 0.01), the convexity error would be −4. Remember that these data are outside the mixing polytope and therefore have a negative average end-member contribution. Logically 'good' models have a small convexity error: the program performs a maximum of 1000 iterations or stops after having reached a convexity error of −6 (equal to for example 1% of the data with an average negative end-member contribution of 1%). The algorithm accepts that some data points remain outside the mixing polytope in order to ensure a stable and interpretable solution. The algorithm converges because each mixing polytope encloses that of the previous iteration. The convexity error is therefore smaller for each successive iteration step.

Further, the coefficient of determination (r^2) between the model and the input data is calculated for end-member models with an increasing number of end members. Obviously 'good' models have a high coefficient of determination. If r^2 is plotted against the corresponding end-member number, the break-in-slope provides a useful guideline for the optimum number of end members: the steeper slope at the low number of end members is considered 'information' and the almost-horizontal slope at the higher number of end members is 'interpretational noise', analogous to the scree-test regularly used in exploration geology. In this 'noise end', some end members differ only minutely from each other which often makes little sense in terms of interpretation: there is a serious risk that

the dataset can be over-interpreted. In a way, this reflects the inherent natural variability of the end members; it is better to merge similar end members into a single end member with essentially the same meaning. Another case that bears the risk of over-interpretation is the following: if one end member would be represented by (almost) a single sample in the data without being present at least at some level in the others, there is a fair chance that that sample is anomalous in some way (it is so remarkable that it constitutes an end member). It should be discarded from the dataset and, after rerunning the analysis, both sets of solutions should be checked for consistency and interpretability.

Above all, end members must be geologically interpretable as emphasized by Weltje (1997). In the present case, end members must be understandable in terms of IRM acquisition curves of individual magnetic minerals or their combinations that subsequently can be tied to processes. Odd-shaped and noisy end-member IRM acquisition curves are unrealistic and the corresponding model should be discarded. Only meaningful end members should be linked to processes such as provenance area, lithological composition, remagnetization, etc.

Input IRM acquisition curves

Attention should be paid to the input IRM acquisition curves because the end-member model algorithm is sensitive to small and subtle effects. IRM acquisition curves can also be modelled by forward techniques. The cumulative log-Gaussian (CLG) approach (Robertson & France 1994; Kruiver *et al.* 2001) has been applied in a wide variety of settings. The CLG basis function has its limitations however because skewness and kurtosis are not incorporated. Skewness in particular can be inherent to some coercivity distributions (Egli 2003, 2004; Heslop *et al.* 2004) and a skewed generalized Gaussian (SGG) set of basis functions seem to be more appropriate (Egli 2003). However, the interpretation of datasets with both approaches shows large similarities (the effect of kurtosis is often insignificant and skewness can be modelled with an extra very low-coercivity component). It illustrates, however, that a non-parametric technique such as end-member modelling could be preferable as a starting point for the interpretation of IRM acquisition curves as it circumvents selection criteria pertaining to the optimal basis function (Heslop & Dillon 2007). If desired, the forward techniques could be implemented later to constrain the end-member interpretation. The input IRM acquisition curves are therefore determined in line with the criteria to be amenable to so-called IRM component analysis (Kruiver *et al.* 2001; Egli 2003). To minimize deviation from log-normality (Egli 2004; Heslop *et al.* 2004), IRM acquisition curves should be determined from the three-axis alternating field demagnetized starting state with the last demagnetization axis parallel to the IRM acquisition field. In this way, maximum discriminative power is achieved.

In addition, many marls and limestones may have surficially oxidized magnetite particles (Van Velzen & Zijderveld 1995), the magnetic effects of which have a bearing on the shape of IRM acquisition curves because the incipient surficial oxidation hardens the magnetic particles. Annealing at 150 °C undoes the effects of this oxidation (Van Velzen & Zijderveld 1995) and results in much better separated primary and secondary NRM components (e.g. Gong *et al.* 2008). Since remagnetization is often associated with magnetite, it is recommended to apply the annealing before the AF demagnetization and subsequent IRM acquisition (Gong *et al.* 2009*b*). However, when dealing with greigite-bearing remagnetized rocks such as those described by Rowan & Roberts (2006, 2008), 5–10 minutes of annealing at 150 °C might change the greigite properties and is not recommended. Greigite-bearing remagnetizations are not discussed in this contribution, however.

The end-member model algorithm is very sensitive to instrumental bias. The IRM acquisition curves should therefore be measured in a reproducible manner, avoiding large differences in time between field application and IRM measurement in a sample collection to be processed. In this way, short-term viscosity effects are minimized. Pulse magnetizers should also be checked for peak-field reproducibility and potential under-damping.

Case studies

The IRM acquisition curves discussed here are measured with a robotized 2 G DC-SQUID (Direct Current Superconducting QUantum Interference Device) magnetometer (instrumental noise level 3×10^{-12} Am^2) with 'in-line' set-up for IRM acquisition curves up to 700 mT at the Utrecht University (Netherlands) palaeomagnetic laboratory. All data were acquired with the so-called two-position measurement protocol. This allows the best correction for the (slightly varying) contribution of the sample tray. Despite the fact that this variation is very small, the end-member analysis may lead to flawed end members and mixing proportions. In these cases, the entire effort is understandably rather meaningless and may lead to incorrect conclusions and inferences. It must be realized that high-end mathematical algorithms (such as the end-member modelling algorithm) are sensitive to small biases in input data, so extra care must be executed to have really 'clean' input data. The MATLAB

modules used for the calculation and an executable can be found online at: http://www.marum.de/Unmixing_magnetic_remanence_curves_without_a_priori_knowledge.html

The program calculates the solutions between 2 and 9 end members. The following criteria were used as guidelines to decide on the optimal number of end members: (1) r^2 between the input data and the end-member model (Heslop *et al.* 2007) must be >0.8; (2) inclusion of yet another end member provides little extra interpretational value (the equivalent of the scree-test); (3) virtual duplication of end members should be avoided: the limit of interpretational power has been reached; and (4) the program calculates the end-member model by iteration until a stopping convexity error has been reached (set at -6); if that convexity is not reached within 1000 iterations, the convexity error at termination can also be used to judge the quality of the model.

In addition, users must be certain that the entire data variability has been sampled by the input IRM acquisition curves; otherwise, the resulting end members are not representative. This is difficult to check but when end-member models from subsets of the data are essentially the same as those from the complete data array, it can be reasonably assumed that the complete data variability was indeed sampled.

The case studies described below were intended to explore whether end-member modelling could identify remagnetized and non-remagnetized strata in geological situations that were known beforehand. Importantly, this knowledge is not used in the end-member modelling effort, but provides a 'training set'. Importantly, this knowledge is not used in the end-member modelling effort. Instead it provides a 'training set' to investigate the performance of the end-member modelling algorithm in identifying remagnetized rocks. The goal in the longer term is to be able to use end-member modelling as an independent decision tool to diagnose whether or not a rock sequence is remagnetized. This is particularly useful when directional information may not be available (due to complex local tectonics) or is subject to rather large uncertainty (as is the case for many Precambrian rocks).

Organyà Basin (Spain): remagnetized and non-remagnetized limestones

Across the Iberian Peninsula various Mesozoic sedimentary basins occur. Organyà Basin (Fig. 1) is the northernmost basin of the South Central Pyrenees thrust sheets, a piggy-bag series of nappes with the basin as the uppermost structural unit. Its sediments consist of mainly Lower Cretaceous limestones and marls. Marine sedimentation halted during the Cenomanian and nappe stacking began at the end of the Cretaceous and continued throughout the formation of the Pyrenees mountain chain. Triassic Keuper evaporates often acted as décollement.

Most Mesozoic basins in Iberia are remagnetized. Organyà Basin is atypical in the sense that the Cretaceous limestones up to the Barremian are remagnetized, but the Aptian and Albian marls with intercalated limestones contain a primary NRM (Dinarès-Turell & García-Senz 2000; Gong *et al.* 2008). The study of Dinarès-Turell & García-Senz (2000) indicated hysteresis parameters more or less in line with the remagnetized and non-remagnetized trend lines (Channell & McCabe 1994). However, the non-remagnetized samples plot close to the SD region where the diagnostic power of the trend lines is not large. Many samples studied by Gong *et al.* (2008) appeared to yield hysteresis loops subject to a fair amount of uncertainty because of low signals. Organyà Basin therefore constitutes an ideal setting to study the properties of remagnetized limestones and non-remagnetized limestones and marls with IRM acquisition curves and end-member modelling (Gong *et al.* 2009*b*). The rocks are close to each other in space and time and a fair number of samples must be discarded in hysteresis loop analysis.

In their study, Gong *et al.* (2009*b*) examined two sets of IRM acquisition curves of limestones and marls (288 IRM acquisition curves in total). Each set consists of three sites: one of remagnetized limestones, one of non-remagnetized limestones and one of non-remagnetized marls (unfortunately remagnetized marls do not occur in the study area). One set of samples (48 specimens for each of the 3 sites) was annealed at 150 °C before AF demagnetization and subsequent IRM acquisition and the other was not heated before this treatment (48 sister specimens from each of the 3 sites). As more or less anticipated, the annealed samples yielded better discriminative results in the end-member analysis and are discussed here. It appeared that in 16 remagnetized limestones (2 rows of 8 samples), the flux jump correction was incorrectly handled by the magnetometer software. This bug was discovered during measurement of this IRM acquisition series, which was the first to be measured with the automated system, and has since been corrected. After data selection, 32 specimens remained for the remagnetized limestones while all 48 specimens were retained for the two non-remagnetized groups.

At the initial stage the end members were calculated for each individual dataset, that is, the remagnetized (R) and non-remagnetized (NR) limestones, both annealed (Fig. 2). For both datasets, models with three end members were selected (r^2 *c.* 0.75–0.8 on the low side which is considered acceptable). The fourth end member almost duplicates one of the

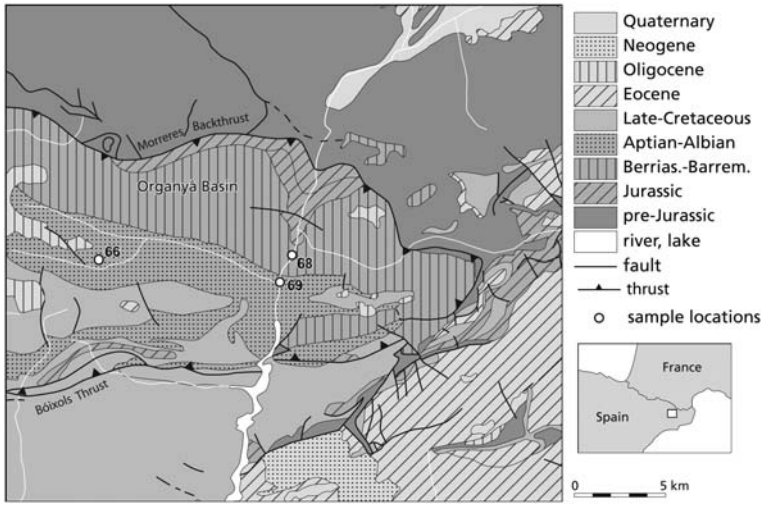

Fig. 1. Simplified geological map of the Organyá Basin with the sites investigated by Gong *et al.* (2009*b*, fig. 1) indicated.

existing end members, risking over-interpretation of the data; models with four or more end members are not considered further. Merging of the data (lowermost panels) shows essentially the same end members (Fig. 2); the entire data variability has therefore been collected and the end members are meaningful.

The shape of the end members indicate a high-coercivity end member labelled EM3 and interpreted to be hematite or goethite (goethite is less likely given its appreciable increase in fields from 200 mT upward already). The two low-coercivity end members are two grain-size distributions of magnetite. Importantly, one saturates at 300–400 mT which is compatible with fine-grained pseudo-single-domain magnetite, labelled EM1. The other low-coercivity end member (EM2) shows an appreciable increase in IRM up 100–200 mT acquisition fields, but does not saturate entirely in the maximum available field of 700 mT. This behaviour is in line with closely spaced very fine, nominally superparamagnetic (SP), magnetically interacting particles often associated with remagnetized limestones (e.g. Suk *et al.* 1993; Sun & Jackson 1994; Katz *et al.* 2000). It is envisaged that, by their non-stoichiometry, partially maghemitized surface layers raise the energy barrier for spin reorientation thus raising the coercivity. Industrial fly ashes show such behaviour in a much more extreme fashion: samples do not saturate at all even in 2 T fields (Dekkers & Pietersen 1992). It was shown via transmission electron microscopy that those samples contained such magnetically interacting fine SP particles in significant amounts. Non-remagnetized limestones should contain EM1 in fairly large amounts while remagnetized limestones contain an appreciable fraction of EM2. Depicted in a ternary plot (Fig. 3) this is indeed the case: end-member modelling successfully discriminates remagnetized and non-remagnetized limestones solely on the basis of magnetic properties. As a rule, non-remagnetized limestones contain a minor contribution of the remagnetized end-member and vice versa so samples may indeed plot in between the two trend lines on the Day plot. EM3 is not relevant for the interpretation of remagnetized v. non-remagnetized limestone. Its contribution is therefore taken out by renormalizing end members 1 and 2 to 100% (Fig. 4). It shows that most samples indeed plot at their expected positions. When the averages (or more exactly, the measures of location) per group with the 95% confidence levels are calculated (including all samples), it appears that the remagnetized and non-remagnetized limestones are significantly different. Because the end-member proportions are closed data, the additive log-ratio transform was used to create a pseudo-open data space for this calculation (Aitchison 1982; Heslop 2009). For example, for a given EM1 this transform is $x = \log [EM1/(1-EM1)]$ and the plotted results are back-transformed. The marl samples appear to have very similar IRM acquisition curves which are perfectly compatible with their non-remagnetized nature: a low contribution of their EM2 and an EM1 that is saturating between 200 and 300 mT.

Case studies in southern Turkey

The amalgamation of the Anatolian–Tauride Block (ATB) in present-day southern Turkey with Eurasia

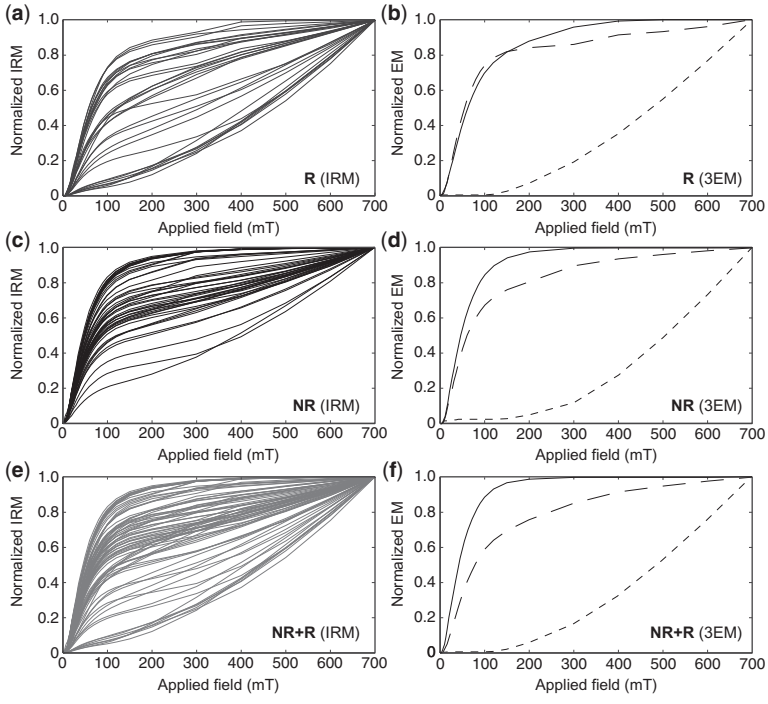

Fig. 2. End-member models for the IRM acquisition curves from the limestone groups that were pre-annealed at 150 °C. (**a**) Normalized IRM acquisition curves from the remagnetized (R) limestones. (**b**) Calculated end members for the remagnetized limestones in the three-end-member model. (**c**) Normalized IRM acquisition curves from the non-remagnetized (NR) limestones. (**d**) End members for the non-remagnetized limestones in the three-end-member model. (**e**) Normalized IRM acquisition curves from the merged dataset of the remagnetized and the non-remagnetized limestones. (**f**) End-members for the three-end-member model of merged pre-annealed limestones. Note the distinctly variable input IRM acquisition curves; the entire variability can be described by three end members. In the end-member diagrams (b, d and f), solid lines indicate the low-coercivity component (end member 1), long dashed lines indicate the low-coercivity component (end member 2) and short dashed lines indicate the high-coercivity component (end member 3) (Gong *et al.* 2009*b*, fig. 3).

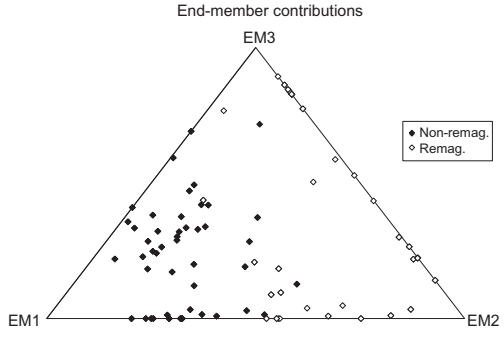

Fig. 3. Ternary plot with the percentages of the three end members in the end-member model from the pre-annealed limestones. End member 1 (EM1) is the down-left apex, end member 2 (EM2) is the down-right apex and end member 3 (EM3) is the top apex. Non-remagnetized (remagnetized) samples are indicated with full (open) diamonds according to their field-based site allocation (Gong *et al.* 2009*b*, fig. 4).

is a topic of intense geological research that has resulted in conflicting models to explain the geological history. The ATB with Cambrian–Tertiary sediments has a Gondwanan affinity and is considered to have rifted apart from Gondwana in the early Mesozoic (e.g. Şengör & Yilmaz 1981). The next two case studies deal with various aspects of this history and examine the remagnetized and non-remagnetized nature of the rocks under study with their direct geological implications. Unfortunately, extended databases of hysteresis properties or other magnetic property data for the study areas are not available. The outcome of the end-member analysis can therefore only be compared to palaeomagnetic directional information. In the Bey Dağlari study, non-remagnetized sediments are analysed while the Taurides study discusses remagnetized strata. The end-member model analysis appears to fully support the geological and palaeomagnetic information as detailed below.

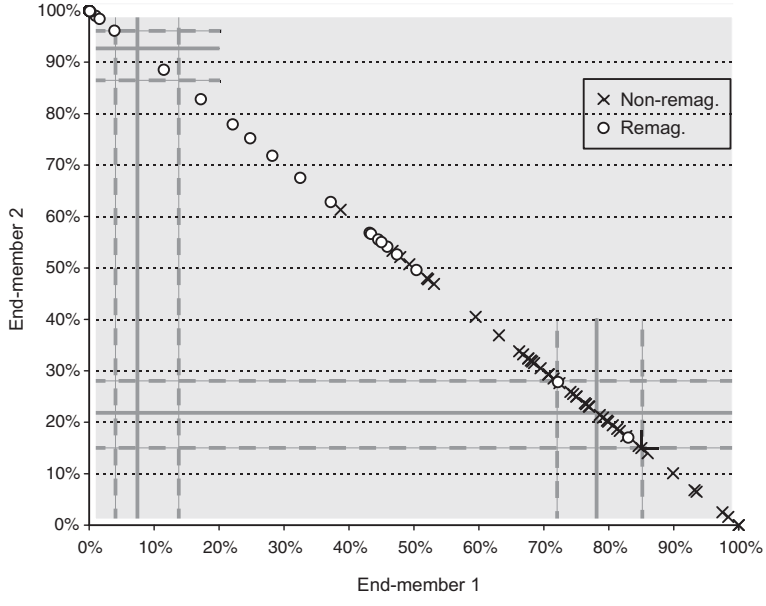

Fig. 4. The contribution of end member 1 v. end member 2 corrected for the (variable) contribution of the high-coercivity end member 3 for the pre-annealed limestone dataset. The open dots indicate the remagnetized data and the crosses denote the non-remagnetized data on the basis of site allocation. Note that these designations are independent of the end-member model calculation. The end-member averages (or measures of location) for the remagnetized and non-remagnetized datasets are indicated with the full lines. The lower and upper bounds of the 95% confidence areas are given with the dashed lines. The log-ratio transform was applied to account for the closed data (see text). Because the data are closed, the end-member 'averages' for each dataset added are 100%: for the non-remagnetized limestones, the average of end member 1 is 78% and thus that of end-member 2 is 22%. For the remagnetized limestones, the averages of end members 1 and 2 are 7% and 93%, respectively. While some individual samples would be classed incorrectly, the group averages are statistically significantly different (Gong *et al.* 2009*b*; fig. 5).

Bey Dağlari: non-remagnetized strata. The first case study involves the analysis of a set of non-remagnetized Miocene sediments from the Bey Dağlari region in southern Turkey (Fig. 5; Van Hinsbergen *et al.* 2010*a*). The results are included in an overall compilation of palaeomagnetic directions across southwestern Turkey to explain oroclinal bending of the eastern branch of the Aegean arc during Miocene times (Van Hinsbergen *et al.* 2010*b*) in relation to the formation of the Menderes Massif metamorphic core complex. This extension was accommodated by thrusting and strike-slip faulting in the so-called Isparta Angle in the Antalya region of southern Turkey. In the then prevailing geodynamic scenario, the Bey Dağlari region has rotated *c.* 25° anticlockwise post-dating a Middle Miocene remagnetization. To test this model, van Hinsbergen *et al.* (2010*a*) studied two Lower Miocene composite sections in the area spanning the period from the Aquitanian unconformity with the Bey Dağlari limestones to approximately the Burdigalian–Langhian boundary. Limestones occur dominantly in the Aquitanian while the Burdigalian primarily consists of blue clays. A positive reversals test, correlatable magnetostratigraphy and the occurrence of inclination shallowing all point to a primary NRM. This was confirmed by the end-member analysis described below. The new palaeomagnetic results indicate that the Bey Dağlari region did not undergo rotation between the late Cretaceous and the late Burdigalian, and rotated *c.* 20° between 16 and 5 Ma. Hence, both limbs of the Aegean orocline rotated more or less coevally (Van Hinsbergen *et al.* 2010*a*).

Forty-nine IRM acquisition curves served as input to calculate the end-member model. Before IRM acquisition the samples were AF demagnetized, but not pre-annealed at 150 °C. The effects of pre-annealing on NRM demagnetization behaviour in the blue clay samples was shown to be insignificant in a pilot series. For this particular dataset, the optimal end-member solution was judged a three end-member model: r^2 is 0.84 and the final convexity level is −3.8. Models with a higher number of end members have only marginally higher r^2; in contrast their convexity level is

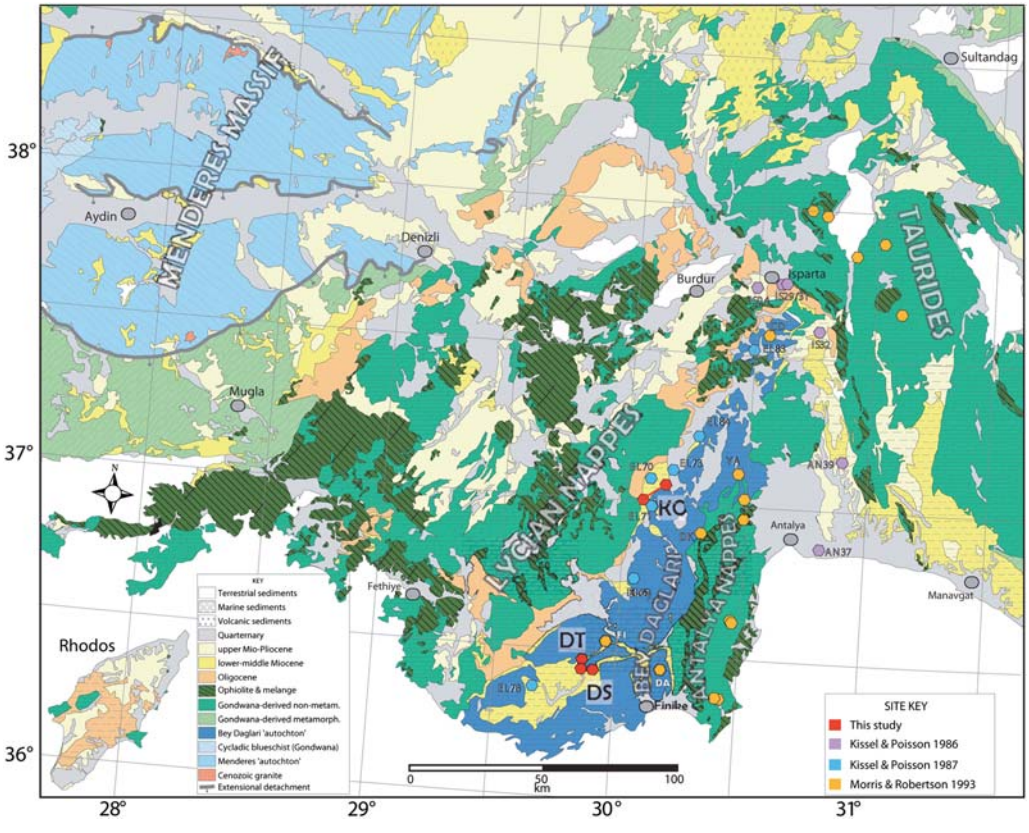

Fig. 5. Geological map of southwestern Turkey. Sample locations of Van Hinsbergen *et al.* (2010*a*) in red. The Lycian Nappes overthrust the Bey Dağlari platform from the NW and the platform is overthrust by the Antalya Nappes from the east. The central Tauride area in the east of this map is the topic of the Meijers *et al.* (2011) study (Van Hinsbergen *et al.* 2010*a*, fig. 2).

worse. The break-in-slope in the curve of r^2 v. the number of end members occurs at three end members. Further, from five end-member solutions onward, at least two of the end members essentially duplicate. The shape of the end members is shown in Figure 6. End member 1 is the comparatively hard SD-style magnetite typical of most limestones. End member 2 represents the softer PSD magnetite that occurs mainly in the blue clays. Note that both saturate at 300–400 mT, in line with their anticipated non-remagnetized nature and the results of Gong *et al.* (2009*b*). Lithological differences are tracked by subtle differences in magnetic properties. In the ternary plot (Fig. 6), samples with high contributions to end members 1 and 2 plot close to the baseline. Limestone samples are black and blue clay samples light grey.

The interpretation of the present end member 3, which has a prominent low-coercivity part and a high-coercivity tail up to 700 mT, is more complicated. The shape of this end member resembles the remagnetized end member in the study of Gong *et al.* (2009*b*), which could imply that the samples with a high contribution of this end member would be remagnetized, as in the dataset of Gong *et al.* (2009*b*). In the present dataset, however, the hematite component is not identified as a separate end member as in the case study of Gong *et al.* (2009*b*). The hematite contribution up to 700 mT is often minute and only occasionally more prominent. The end-member algorithm (that imposes no constraints on the shape of the end members) therefore does not appear to resolve a separate hematite end member.

To constrain the end-member interpretation, Van Hinsbergen *et al.* (2010*a*) turned to a forward modelling approach as a supplementary tool. They utilized IRM acquisition curve coercivity component fits (cf. Kruiver *et al.* 2001). In samples where an appreciable amount of hematite was

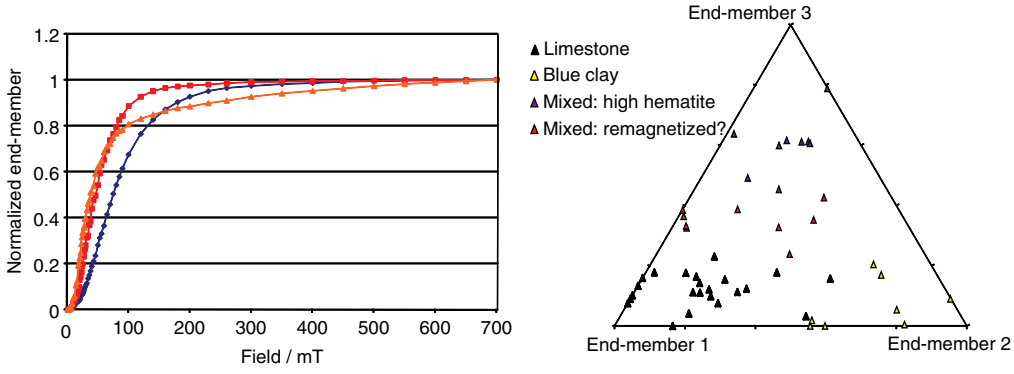

Fig. 6. End-member modelling results of Van Hinsbergen *et al.* (2010*a*). Left panel: the shape of the calculated end members in a three-end-member model. End member (EM) 1 (diamonds) is interpreted as SD magnetite and occurs dominantly in the limestones. EM2 (squares) is softer PSD magnetite and occurs mostly in the blue clays. Both saturate in *c.* 300 mT in line with their non-remagnetized nature. End member 3 (triangles) has a dual meaning (see also main text): it represents either a mixture of magnetite and hematite (in cases where IRM acquisition curve fitting yielded a fair amount of hematite) or the samples could be remagnetized (in cases where IRM acquisition curve fitting yielded a marginal amount of hematite). Right panel: ternary plot with the EM partitioning for each sample. Samples with a substantial hematite content are interpreted as a mixture of magnetite and hematite. In contrast, samples with *c.* 40% of end member 3 but virtually devoid of hematite are possibly remagnetized. These all occur close to the basal unconformity (Van Hinsbergen *et al.* 2010*a*, fig. 13).

required for the IRM component fit, end-member 3 was considered a mixture of soft magnetite and hematite. In samples where the amount of hematite required for the IRM fit is just a few percent, a mixture of magnetite and hematite cannot be the cause for the shape of end member 3. For these samples, the possibility of remagnetization is invoked. These samples almost all appeared to be located within *c.* 5 m from the basal unconformity. It is perfectly conceivable that those samples are actually remagnetized by the action of percolating groundwater using the unconformity as an aquifer. In this study, end member 3 therefore has a dual interpretation: in cases where appreciable hematite was fitted to the IRM acquisition curves, we interpret end member 3 as a mixture of magnetite and hematite; the samples probably carry a primary NRM as well. These samples have the highest end member 3 contribution. In those samples with raised end member 3 contributions but with hardly any hematite required in the IRM curve fits, the possibility of remagnetization cannot be excluded. Note that the latter group constitutes only a very small fraction of the total amount of samples. The vast majority of the samples (>95%) which determine the rotation and magnetic polarity of the sections were taken from blue clay, which provides no reason at all to suspect remagnetization.

Taurides: remagnetized strata. The Taurides sedimentary sequences of Cambrian–Tertiary age is mostly composed of shallow marine platform-type carbonates (e.g. Şengör & Yilmaz 1981; Mackintosh & Robertson 2009). The Taurides consist of several isopic units (Fig. 7) that are stacked as nappe sequences mainly during the late Cretaceous–Oligocene (Andrew & Robertson 2002; Özer *et al.* 2004). Palaeogeographically, these isopic zones include (from south to north) the Antalya, Alanya, Geyikdağı, Aladağ, Bolkardağı and Bozkır units. The Geyikdağı unit is structurally the lowest and relatively autochtonous unit (Fig. 7). Because of its similar structural position and stratigraphy, the unmetamorphosed and mildly deformed Bey Dağlari unit is generally considered as the lateral equivalent of the parautochthonous Geyikdağı unit. The tectonostratigraphic stacking was followed by the aforementioned middle–late Miocene anticlockwise vertical axis rotation in the western limb of the Isparta Angle (Kissel & Poisson 1987; Morris & Robertson 1993) determined for Lycian Nappes and Bey Dağlari region.

Meijers *et al.* (2011) conducted their study in the central Taurides, the eastern limb of the Isparta Angle. Here, late Cretaceous–Eocene compression formed the fold and thrust belt, structurally equivalent to the Lycian Nappes in the west. The stacking however took place at different times in each domain. The central Taurides fold and thrust belt is unconformably overlain by Miocene marine and terrestrial deposits.

This study of remagnetized rocks involved the end-member analysis of 174 IRM acquisition curves. The study was focused on the long Seydişehir

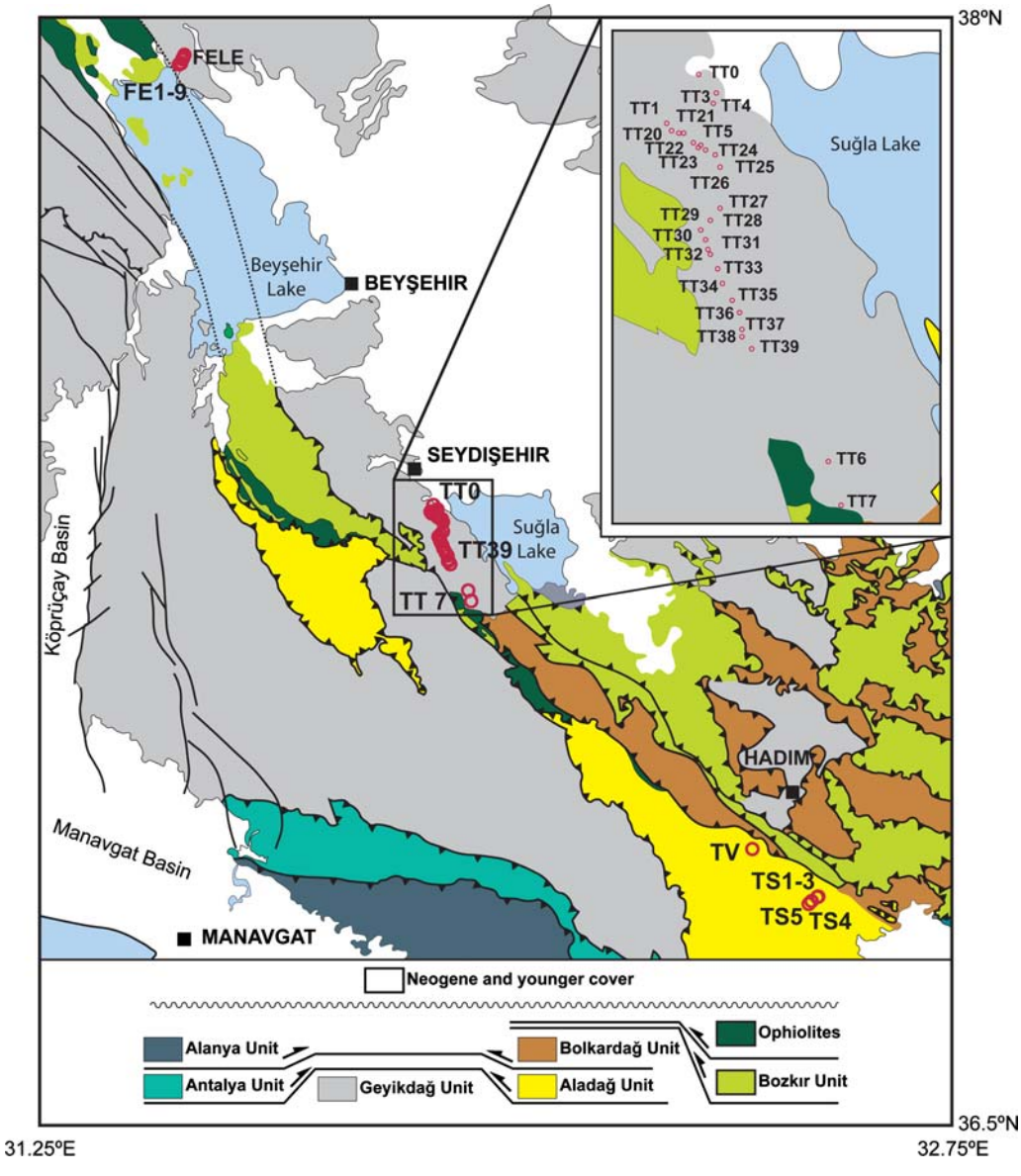

Fig. 7. Geological map of the study area of Meijers *et al.* 2011. In the lowermost part the schematized tectonostratigraphic build-up of the nappe sequence is provided. The discussion here is confined to the Seydişehir section (labelled TT; Meijers *et al.* 2011, fig. 3).

section (*c.* 2000 m stratigraphy) that consists of many rock types (limestones, sandy/shaly limestones, dolomitic limestones). Before IRM acquisition, the specimens were pre-heated to a temperature of 150 °C in a magnetically shielded oven and AF demagnetized according to the IRM acquisition curve protocol. The IRM was acquired in 57 steps up to 700 mT with the in-house developed robotized magnetometer.

First, data subsets were subjected to the end-member analysis. The merged data showed essentially the same end members so the entire data variability was included in the analysis and its outcome is not input-dependent. Meijers *et al.* (2011) propose either a two- or a three-end-member model. Coefficients of determination are 0.87 and 0.90 and the convexities at termination −5.00 and −2.50, respectively. From four end members onwards,

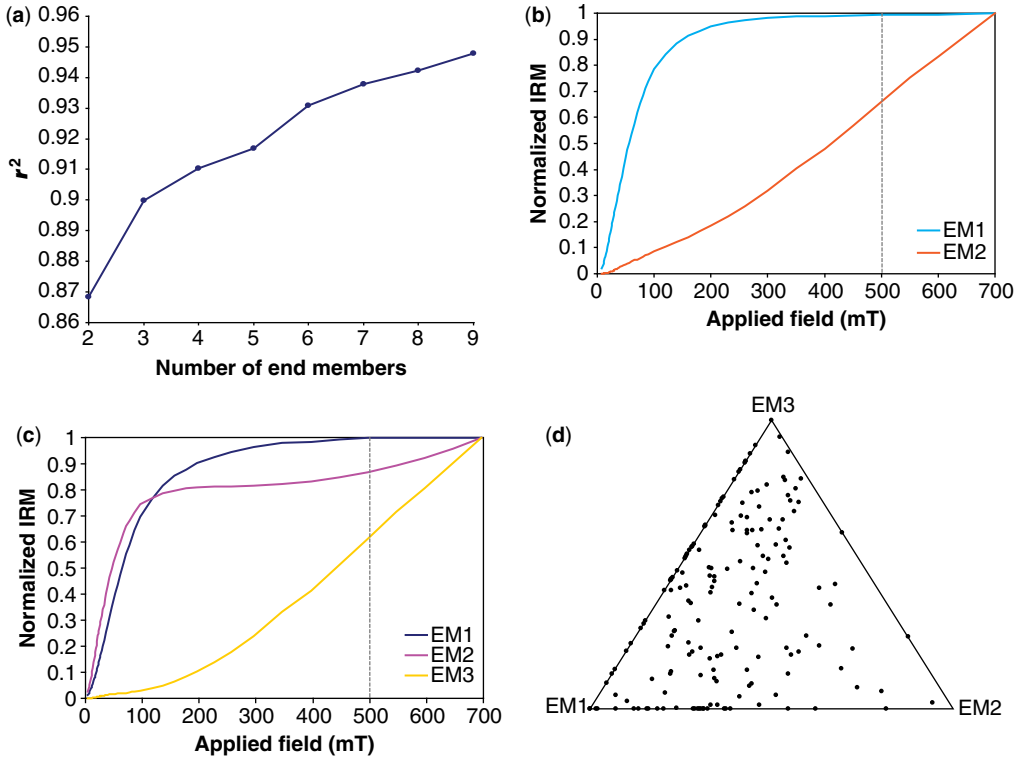

Fig. 8. (**a**) Plot of r^2 v. end-member (EM) number. A three-end-member model is preferable; in the five-end-member solution duplication of end members occurs. (**b**, **c**) End members for the normalized IRM acquisition curves for the (b) two and (c) three end-member models. (**d**) Ternary plot showing for each sample the percentages of the end members (EM) in the three-end-member model (Meijers *et al*. 2011, fig. 8).

duplication of end members occurs; evidently, the data become over-interpreted. A two-end-member model yields a discrimination in a magnetite (with a remagnetized nature) and a hematite end member (Fig. 8). Indeed, samples with a higher hematite end-member proportion also have a higher hematite contribution in (forward) IRM component fitting. The three-end-member model is preferred (with EM1, 2, 3) because it can be interpreted as reflecting lithological grouping and it represents the break-in-slope of the r^2 v. number-of-end-members curve (Fig. 8a). The two 'magnetite' end members in that model both have a remagnetized nature.

End-member shapes here reflect magnetic minerals. NRM directions (Meijers *et al.* 2011) are of dual polarity (without any correlation to the GPTS) and represent Early Tertiary directions for the ATB. The EM distribution and the polarity of the samples appear to be unrelated; the end members reflect magnetic processes and properties, not geomagnetic field behaviour. EM3 (light grey in Fig. 8) represents hematite and samples with a high proportion of EM3 indeed show a considerable contribution of a high-coercivity IRM fraction in the forward log-Gaussian approach. EM1 (black in Fig. 8) is logically interpreted as representing magnetite. The SIRM of this end member is reached at 500 mT, a notably high field for 'classic' magnetite that typically reaches SIRM at 200–300 mT. Remagnetized magnetite particle suites can however reach saturation at much higher fields, supporting the remagnetized nature of the Tauride rocks under study.

The majority of the samples are mixtures of EM1 and EM3 in variable proportions (Fig. 8) with only minor contributions of EM2 (dark grey). As in the Van Hinsbergen *et al.* (2010*a*) study, the interpretation of end members can be complicated. This applies to EM2 in this case, which can be considered a mixture of (relatively soft) magnetite with a tail of hematite. This is supported by the slightly sandy nature of the limestones with an appreciable EM2 contribution. Alternatively, it could be associated with aggregates of ultrafine ferrimagnetic

particles with a composition similar to magnetite which do not saturate at 700 mT. The EM2/EM3 ratio is substantially higher in dolomitic limestones and supports this latter interpretation. In general, dolomitic limestones are associated with high EM1 and low EM3 contributions, which make the existence of hematite tails in another end member unlikely (mathematically, its existence would not be likely either). Both EM1 and EM2 represent remagnetized magnetites.

Widespread Miocene remagnetization in the Bey Dağlari region and Lycian Nappes was negated by Van Hinsbergen *et al.* (2010*a*, *b*). For the Lycian Nappes this would concur with their high structural position. However, the evidence for remagnetization affecting the Antalya Nappes presented by Morris & Robertson (1993) remains firm.

In the Taurides, the oldest and structurally highest nappes are the 'ophiolites' (Bozkır, Antalya and Lycian) that are widespread across southern Turkey with metamorphic soles of 90–95 Ma (e.g. Çelik *et al.* 2006). This is older than the maximum age for remagnetization (palaeolatitude and reversed polarity are incompatible with the Cretaceous normal polarity superchron). After the emplacement of the ophiolites, folding and thrusting of the ATB eventually led to the development of the fold and thrust belt in the early Eocene (Özgül 1983). This implies that the remagnetization is more likely related to folding and thrusting during the Paleocene–early Eocene rather than to the ophiolite emplacement at $<$95–90 Ma. Based on the similar inclinations from all sites after tilt correction, remagnetization probably occurred before tilting or during the early stages of tilting, that is, in the early stages of folding and thrusting. This is supported by the small-circle-intersection method (Waldhör & Appel 2006) that shows best grouping at an early stage of folding (Meijers *et al.* 2011). Folding and thrusting could also be a candidate for remagnetization in the rocks sampled by Morris & Robertson (1993) in the Antalya Nappes in the Bey Dağlari region, which underwent nappe stacking during the same time interval (Juteau *et al.* 1977; Robertson & Woodcock 1981; Çelik *et al.* 2006).

Large amounts of external orogenic fluids are considered unlikely given the absence of related low-temperature Mississippi Valley Type ores in the region. Magnetite formation as a result of diagenetic reactions involving clay minerals is deemed more plausible. Influence of pressure solution, although equivocal in remagnetization processes (Evans *et al.* 2003; Elmore *et al.* 2006), cannot be excluded because stylolites are often observed. The Seydişehir section shows continuous sedimentation into the Palaeocene and lower Eocene foreland basin deposits. The timing of remagnetization is therefore likely Eocene, and may have influenced all Eocene and older fold and thrust rocks in the central Taurides axis.

Geochemical analysis and K–Ar dating of clay mineral suites may offer further clues to the remagnetization process in the Taurides. The approach described by Zwing *et al.* (2009) is particularly attractive. In their study of the NE Rhenish Massif in Germany, Zwing *et al.* (2009) were able to relate an older diagenetic illite suite (348 $\pm$ 7 Ma) to a regional mild thermal event that is interpreted to have caused remagnetization by action of fluids. A younger diagenetic illite suite (324 $\pm$ 3 Ma) was related to deformation. That younger event has overprinted earlier remagnetized NRM but not the illite that was already formed. If illite formation age trends with their geochemical signature can be established for the Taurides, this undoubtedly contributes to a robust unravelling of tectonostratigraphic, deformation and burial temperature arguments for that setting.

Conclusions and prospects

It is clear that proper identification of remagnetized and non-remagnetized rocks is crucial to correctly understand the geological development of mountain belts, illustrated here with examples from the central Taurides area. End-member modelling is helpful to identify remagnetized and non-remagnetized limestones. End members reflect processes that have resulted in certain specific magnetic mineral signatures. When interpreting the end-member model options incorporation of forward techniques, such as log-Gaussian IRM acquisition curve fitting, is recommended in conjunction with the mathematical criteria to judge end-member solutions. A foremost criterion, however, is that any interpretation must make sense in the general geological context of the study area. Current end-member studies have concentrated on limestones. It is desirable that the 'training set', which is presently rather small, is enlarged by including more test case studies that also include other lithologies. In the longer term, this may result in the possibility of identifying chemical remagnetization for groups of samples and, in some cases, even on an individual sample basis (as for the samples close to the basal unconformity in the Van Hinsbergen *et al.* 2010*a* study) without having to consider palaeomagnetic directional behaviour.

The IRM acquisition data reviewed here were acquired with support of the Earth and Life Science Division of the Netherlands Science Foundation and the Netherlands Research Centre for Integrated Solid Earth Science (ISES).

References

Aitchison, J. 1982. The statistical analysis of compositional data. *Journal of the Royal Statistical Society Series B*, **44**, 139–177.

Andrew, T. & Robertson, A. H. F. 2002. The Beysehir–Hoyran–Hadim Nappes: genesis and emplacement of Mesozoic marginal and oceanic units of the northern Neotethys in southern Turkey. *Journal of the Geological Society, London*, **159**, 529–543.

Bezdek, J. C., Erhlich, R. & Full, W. 1984. FCM: the fuzzy c-means clustering algorithm. *Computers & Geosciences*, **10**, 191–203.

Çelik, Ö. F., Delaloyle, M. F. & Feraud, G. 2006. Precise $^{40}Ar-^{39}Ar$ ages from the metamorphic sole rocks of the Tauride Belt Ophiolites, southern Turkey: implications for the rapid cooling history. *Geological Magazine*, **143**, 213–227.

Channell, J. E. T. & McCabe, C. 1994. Comparison of magnetic hysteresis parameters of unremagnetized and remagnetized limestones. *Journal of Geophysical Research*, **99**, 4613–4623.

Day, R., Fuller, M. D. & Schmidt, V. A. 1977. Hysteresis properties of titanomagnetites: grain size and composition dependence. *Physics of the Earth and Planetary Interiors*, **13**, 260–267.

Dekkers, M. J. & Pietersen, H. S. 1992. Magnetic properties of low-Ca flyash: a rapid tool for Fe-assessment and a proxy for environmental hazard. *In*: Glasser, F. P. *et al.* (eds) *Advanced Cementitious Systems: Mechanisms and Properties*. Materials Research Society Symposium Proceedings, **245**, 34–47, doi: http://dx.doi.org/10.1557/proc-245-37.

Dinarès-Turell, J. & García-Senz, J. 2000. Remagnetization of Lower Cretaceous limestones from the southern Pyrenees and relation to the Iberian plate geodynamic evolution. *Journal of Geophysical Research*, **105**, 19 405–19 418.

Dunlop, D. J. 2002*a*. Theory and application of the Day plot (M_{rs}/M_s v. H_{cr}/H_c) 1. Theoretical curves and tests using titanomagnetite data. *Journal of Geophysical Research*, **107**, doi: 10.1029/2001JB000486.

Dunlop, D. J. 2002*b*. Theory and application of the Day plot (M_{rs}/M_s versus H_{cr}/H_c): 2. Application to data for rocks, sediments, and soils. *Journal of Geophysical Research*, **107**, 2057, doi: 10.1029/2001JB000487.

Egli, R. 2003. Analysis of the field dependence of remanent magnetization curves. *Journal of Geophysical Research*, **108**, 2081.

Egli, R. 2004. Characterization of individual rock magnetic components by analysis of remanence curves. 2. Fundamental properties of coercivity distributions. *Physics and Chemistry of the Earth*, **29**, 851–867.

Elmore, R. D., Lee-Egger Foucher, J., Evans, M., Lewchuk, M. & Cox, M. 2006. Remagnetization of the Tonoloway Formation and the Helderberg Group in the Central Appalachians: testing the origin of syntilting magnetizations. *Geophysical Journal International*, **166**, 1062–1076, doi: 10.1111/j.1365-246X.2006.02875.x.

Evans, M. A. & Elmore, R. D. 2006. Fluid control of localized mineral domains in limestone pressure solution structures. *Journal of Structural Geology*, **28**, 284–301.

Evans, M. A., Lewchuk, M. T. & Elmore, R. D. 2003. Strain partitioning of deformation mechanisms in limestones: examining the relationship of strain and anisotropy of magnetic susceptibility (AMS). *Journal of Structural Geology*, **25**, 1525–1549.

Font, E., Trindade, R. I. F. & Nédélec, A. 2006. Remagnetization in bituminous limestones of the Neoproterozoic Araras Group (Amazon craton): hydrocarbon maturation, burial diagenesis or both? *Journal of Geophysical Research*, **111**, B06204.

Gong, Z., Langereis, C. G. & Mullender, T. A. T. 2008. The rotation of Iberia during the Aptian and the opening of the Bay of Biscay. *Earth and Planetary Science Letters*, **273**, 80–93.

Gong, Z., van Hinsbergen, D. J. J. & Dekkers, M. J. 2009*a*. Diachronous pervasive remagnetization in northern Iberian basins during Cretaceous rotation and extension. *Earth and Planetary Science Letters*, **284**, 292–301, doi: 10.1016/j.epsl.2009.04.039.

Gong, Z., Dekkers, M. J., Heslop, D. & Mullender, T. A. T. 2009*b*. End-member modelling of isothermal remanent magnetization (IRM) acquisition curves: a novel approach to diagnose remagnetization. *Geophysical Journal International*, **178**, 693–701.

Heslop, D. 2009. Calculating descriptive statistics for the S-ratio. *Geophysical Journal International*, **178**, 159–161, doi: 10.1111/j.1365-246X.2009.04175.x.

Heslop, D. & Dillon, M. 2007. Unmixing magnetic remanence curves without a priori knowledge. *Geophysical Journal International*, **170**, 556–566.

Heslop, D., McIntosh, G. & Dekkers, M. J. 2004. Using time and temperature dependant Preisach models to investigate the limitations of modelling isothermal remanent magnetisation curves with cumulative log Gaussian functions. *Geophysical Journal International*, **157**, 55–63.

Heslop, D., Witt, A., Kleiner, T. & Fabian, K. 2006. The role of magnetostatic interactions in sediment suspensions. *Geophysical Journal International*, **165**, 775–785.

Heslop, D., Von Dobeneck, T. & Höcker, M. 2007. Using non-negative matrix factorization in the 'unmixing' of diffuse reflectance spectra. *Marine Geology*, **241**, 63–78.

Juteau, T., Nicolas, A., Dubessey, J., Fruchard, J. C. & Bouchez, J. L. 1977. Structural relationships in the Antalya Complex, Turkey: possible model for an oceanic ridge. *Geological Society of America*, **88**, 1740–1748.

Katz, B., Elmore, R. D., Cogoini, M., Michael, H. E. & Ferry, S. 2000. Associations between burial diagenesis of smectite, chemical remagnetization, and magnetite authigenesis in the Vocontian trough, SE France. *Journal of Geophysical Research*, **105**, 851–868.

Kent, D. V. 1985. Thermoviscous remagnetization in some Appalachian limestones. *Geophysical Research Letters*, **12**, 805–808.

Kent, D. V. & Opdyke, N. D. 1985. Multicomponent magnetizations from the Mississippian Mauch Chunk Formation of the central Appalachians and their tectonic implications. *Journal of Geophysical Research*, **90**, 5371–5383.

Kissel, C. & Poisson, A . 1987. Etude paléomagnétique préliminaire des formations cénozoïques des BeyDağlari

(Taurides occidentales, Turquie). *Comptes Rendus de l'Académie des Sciences, Paris*, **304**, Serie II, 343–348.

Kruiver, P. P., Dekkers, M. J. & Heslop, D. 2001. Quantification of magnetic coercivity components by the analysis of acquisition curves of isothermal remanent magnetization. *Earth and Planetary Science Letters*, **189**, 269–276.

Lanci, L. & Kent, D. V. 2003. Introduction of thermal activation in forward modeling of hysteresis loops for single-domain magnetic particles and implications for the interpretation of the Day diagram. *Journal of Geophysical Research*, **108**, 2148, doi: 10.1029/2001JB000944.

Mackintosh, P. W. & Robertson, A. H. F. 2009. Structural and sedimentary evidence from the northernmargin of the Tauride platformin south central Turkey used to test alternative models of Tethys during Early Mesozoic time. *Tectonophysics*, **473**, 149–172.

McCabe, C. & Elmore, R. D. 1989. The occurrence of origin of late Paleozoic remagnetization in the sedimentary rocks of North America. *Reviews of Geophysics*, **27**, 471–494.

McCabe, C., Van der Voo, R., Peacor, D. R., Scotese, C. R. & Freeman, R. 1983. Diagenetic magnetite carries ancient yet secondary remanence in some Paleozoic sedimentary carbonates. *Geology*, **11**, 221–223.

Meijers, M. J. M., van Hinsbergen, D. J. J., Dekkers, M. J., Altiner, D., Kaymakci, N. & Langereis, C. G. 2011. Pervasive Palaeogene remagnetization of the central Taurides fold-and-thrust belt (southern Turkey) and implications for rotations in the Isparta Angle. *Geophysical Journal International*, **184**, 1090–1112, doi: 10.1111/j.1365-246X.2010.04919.x.

Molina-Garza, R. S. & Zijderveld, J. D. A. 1996. Paleomagnetism of Paleozoic strata, Brabant and Ardennes Massifs, Belgium: implications of prefolding and postfolding Late Carboniferous secondary magnetizations for European polar wander. *Journal of Geophysical Research*, **101**, 15 799–15 818.

Morris, A. & Robertson, A. H. F. 1993. Miocene remagnetisation of carbonate platform and Antalya Complex units within the Isparta Angle, SW Turkey. *Tectonophysics*, **220**, 243–266.

Oliva-Urcia, B., Pueyo, E. L. & Larrasoaña, J. C. 2008. Magnetic reorientation induced by pressure solution: a potential mechanism for orogenic-scale remagnetizations. *Earth and Planetary Science Letters*, **265**, 524–530.

Özer, E., Koç, H. & Özsayar, T. Y. 2004. Stratigraphical evidence for the depression of the northern margin of the Menderes–Tauride Block (Turkey) during the Late Cretaceous. *Journal of Asian Earth Sciences*, **22**, 401–412.

Özgül, N. 1983. Stratigraphy and tectonic evolution of the Central Taurides. *In*: Tekeli, O & Göncüöglü, C. (eds) *Geology of the Taurus Belt*. International Symposium, Mineral Research and Exploration Inst., 1983 September 26–29, Ankara. Geological Society of Turkey and the Mineral Research and Exploration Institute, Ankara, 78–90.

Perroud, H. & Van der Voo, R. 1984. Secondary magnetizations from the Clinton-type iron ores of the Silurian Red Mountain Formation, Alabama. *Earth and Planetary Science Letters*, **67**, 391–399.

Prins, M. A., Bouwer, L. M. *et al.* 2002. Ocean circulation and iceberg discharge in the glacial North Atlantic: inferences from unmixing of sediment size distributions. *Geology*, **30**, 555–558.

Robertson, D. J. & France, D. E. 1994. Discrimination of remanence carrying minerals in mixtures, using isothermal remanent magnetization acquisition curves. *Physics of the Earth and Planetary Interiors*, **82**, 223–234.

Robertson, A. H. F. & Woodcock, N. H. 1981. Alakir Çay group, Antalya Complex, SW Turkey: a deformed Mesozoic carbonate margin. *Sedimentary Geology*, **30**, 95–131.

Rowan, C. J. & Roberts, A. P. 2006. Magnetite dissolution, diachronous greigite formation, and secondary magnetizations from pyrite oxidation: unravelling complex magnetizations in Neogene marine sediments from New Zealand. *Earth and Planetary Science Letters*, **241**, 119–137.

Rowan, C. J. & Roberts, A. P. 2008. Widespread remagnetizations and a new view of Neogene tectonic rotations within the Australia-Pacific plate boundary zone, New Zealand. *Journal of Geophysical Research*, **113**, B03103, doi: 10.1029/2006JB004594.

Rowan, C. J., Roberts, A. P. & Broadbent, T. 2009. Reductive diagenesis, magnetite dissolution, greigite growth and paleomagnetic smoothing in marine sediments: a new view. *Earth and Planetary Science Letters*, **227**, 223–235.

Şengör, A. M. C. & Yilmaz, Y. 1981. Tethyan evolution of Turkey: a plate tectonic approach. *Tectonophysics*, **75**, 181–241.

Stearns, C. & Van der Voo, R. 1987. A paleomagnetic reinvestigation of the Upper Devonian Perry Formation: evidence for late Paleozoic remagnetization. *Earth and Planetary Science Letters*, **86**, 27–38.

Suk, D., Van der Voo, R. & Peacor, D. R. 1993. Origin of magnetite responsible for remagnetization of early Paleozoic limestones of NewYork state. *Journal of Geophysical Research*, **98**, 419–434.

Sun, W. & Jackson, M. 1994. Scanning electron microscopy and rock magnetic studies of magnetic carriers in remagnetized early Paleozoic carbonates from Missouri. *Journal of Geophysical Research*, **99**, 2935–2942.

Van der Voo, R. & Torsvik, T. H. 2012. The history of remagnetization of sedimentary rocks: deception, developments, discoveries. *In*: Elmore, R. D., Muxworthy, A. R., Aldana, M. M. & Mena, M. (eds) *Remagnetization and Chemical Alteration of Sedimentary Rocks*. Geological Society, London, Special Publications, **371**, first published online 26 June 2012, http://dx.doi.org/10.1144/SP371.2

Van der Voo, R., Stamatakos, J. A. & Parés, J. M. 1997. Kinematic constraints on thrust-belt curvature from syndeformational magnetizations in the Lagos del Valle syncline in the Cantabrian Arc, Spain. *Journal of Geophysical Research*, **102**, 10 105–10 120.

Van Hinsbergen, D. J. J., Dekkers, M. J. & Koç, A. 2010*a*. Testing Miocene Remagnetization of Bey Dağlari: timing and amount of Neogene Rotations in SW Turkey. *Turkish Journal of Earth Sciences*, **19**, 123–156, doi: 10.3906/yer-0904-1.

VAN HINSBERGEN, D. J. J., DEKKERS, M. J., BOZKURT, E. & KOOPMAN, M. 2010*b*. Exhumation with a twist: paleomagnetic constraints on the evolution of the Menderes metamorphic core complex (western Turkey). *Tectonics*, **29**(TC3009), doi: 10.1029/2009TC002596.

VAN VELZEN, A. J. & ZIJDERVELD, J. D. A. 1995. Effects of weathering on single domain magnetite in early Pliocenemarls. *Geophysical Journal International*, **121**, 267–278.

WALDHÖR, M. & APPEL, E. 2006. Intersections of remanence small circles: new tools to improve data processing and interpretation in palaeomagnetism. *Geophysical Journal International*, **166**, 33–45.

WEIL, A. B. & VAN DER VOO, R. 2002. Insights into the mechanism for orogen related carbonate remagnetization from growth of authigenic Fe-oxide: a SEM and rock magnetic study of Devonian carbonates from northern Spain. *Journal of Geophysical Research*, **107**, 2063, doi: 10.1029/2001JB000200.

WEIL, A. B., VAN DER VOO, R., VAN DER PLUIJM, B. A. & PARÉS, J. M. 2000. Unraveling the timing and geometric characteristics of the Cantabria–Asturias Arc (northern Spain) through paleomagnetic analysis. *Journal of Structural Geology*, **22**, 735–756.

WELTJE, G. J. 1997. End-member modelling of compositional data: numerical–statistical algorithms for solving the explicit mixing problem. *Journal of Mathematical Geology*, **29**, 503–549.

ZEGERS, T. E., DEKKERS, M. J. & BAILLY, S. 2003. Late Carboniferous to Permian remagnetization of Devonian limestones in the Ardennes: role of temperature, fluids, and deformation. *Journal of Geophysical Research*, **108**, 2357–2376.

ZWING, A., BACHTADSE, V. & SOFFEL, H. C. 2002. Late Carboniferous remagnetisation of Palaeozoic rocks in the NE Rhenish Massif, Germany. *Physics and Chemistry of the Earth*, **27**, 1179–1188.

ZWING, A., CLAUER, N., LIEWIG, N. & BACHTADSE, V. 2009. Identification of remagnetization processes in Paleozoic sedimentary rocks of the northeast Rhenish Massif in Germany by K-Ar dating and REE tracing of authigenic illite and Fe oxides. *Journal of Geophysical Research*, **114**, 1, B06104, doi: 10.1029/2008JB006137.